Algorithm Design and Performance Analysis of Target Localization Using Mobile Underwater Acoustic Array Networks

Ruoyu Su, Zijun Gong, *Member, IEEE*, Cheng Li, *Senior Member, IEEE*, and Xuemin Shen, *Fellow, IEEE*

***Abstract*—Space-air-ground-sea integrated network, as a promising networking paradigm for the sixth generation (6 G) communications, connects satellite networks, aerial networks, terrestrial networks, and marine networks. As a fundamental application of marine networks, efficient target localization in the ocean is significant for many marine and underwater applications, including oceanic environmental monitoring, subsea resource exploration, and navigation safety. In this paper, to bring more scalability and feasibility of underwater localization, a mobile underwater acoustic array network is utilized to locate underwater moving targets by leveraging linear frequency modulated (LFM) signals. In the mobile underwater acoustic network, one node is constantly broadcasting LFM signals. Based on the reflected signals received by other nodes, a method that jointly utilizes the propagation delay and the Doppler effect is proposed to simultaneously estimate the position and the velocity of the moving target. Specifically, a two-phase iterative algorithm with low computational complexity is designed to improve the estimation accuracy. Closed-form expressions of positioning and velocity estimation error are also presented. Performance evaluation shows that the proposed method clearly outperforms the least squares based approach. Moreover, the estimation accuracy of the proposed method can approach the Cramér-Rao low bound (CRLB) within two iterations. Decently good localization and velocity estimation error performance can be achieved even with an array network formed by a small number of nodes.**

***Index Terms*—Localization, best linear unbiased estimator, mobile underwater acoustic array network, space-air-ground-sea integrated network.**

Manuscript received 22 December 2021; revised 5 June 2022; accepted 21 September 2022. Date of publication 4 October 2022; date of current version 13 February 2023. This work was supported in part by the National Natural Science Foundation of China under Grant 62201162, in part by the Natural Science Foundation of Jiangsu Province under Grant BK20190733, in part by the NUPTSF under Grant NY219166, in part by the Natural Sciences and Engineering Research Council of Canada under Grant RGPIN-2018-03792, in part by the InnovateNL SensorTECH under Grant 5404-2061-101, and in part by the Project Localization and Tracking System for Internet of Underwater Things. The review of this article was coordinated by Prof. Honggang Wang. *(Corresponding author: Cheng Li.)*

Ruoyu Su is with the School of Internet of Things, Nanjing University of Posts and Telecommunications, Nanjing 210003, China (e-mail: suruoyu@njupt.edu.cn).

Zijun Gong is with the IOT Thrust, Hong Kong University of Science and Technology (Guangzhou), Guangzhou, Guangdong 511400, China, and also with the Department of Electrical and Computer Engineering, Hong Kong University of Science and Technology, Hong Kong, SAR, China (e-mail: gongzijun@ust.hk).

Cheng Li is with the Faculty of Engineering and Applied Science, Memorial University of Newfoundland, A1B 3X5 St. John's, NL, Canada (e-mail: licheng@mun.ca).

Xuemin Shen is with the Department of Electrical and Computer Engineering, University of Waterloo, Waterloo, ON N2L 3G1, Canada (e-mail: sshen@uwaterloo.ca).

Digital Object Identifier 10.1109/TVT.2022.3211830

I. Introduction

Compared with the fifth generation (5 G) communication network, the sixth (6 G) communication network is conceived with ultra large network coverage, ultra high density connections, and ultra high frequency bandwidth in the next coming years [1], [2]. To achieve these novel performance, the space-air-ground-sea integrated network emerges as a new and promising architecture to connect satellite networks, aerial networks, terrestrial networks, and marine networks [3], [4], [5]. As an indispensable part of the space-air-ground-sea integrated network in 6 G, the marine network exploits underwater acoustic array networks as the backbone to achieve the wide-range of marine applications, such as marine environment monitoring, resource exploration, and underwater localization and tracking [6]. It is worth noting that the localization and tracking have attracted great interests from both academia and industry in recent years, where the objects may include vessels, marine animal, iceberg, and marine pollutant [4], [6].

In general, depending on various scenarios and different applications, active and passive sonar systems can be used to accomplish localization, navigation, and remote-sensing objectives [7]. The passive sonar system is considered to be an efficient solution to locate objects with self-generated sounds. However, a substantial number of objects that threaten the safety of vessels do not actively generate any sound signal [8]. Active sonar system, on the other side, is able to detect and locate silent objects by utilizing its own probing signals. As shown in Fig. 1, an active mobile sonar system is formed via the collaborative work of several mobile nodes, including the autonomous underwater vehicles (AUVs), remotely operated vehicles (ROVs), and gliders [9], [10], [11]. For example, when a mobile node keeps transmitting acoustic probing signals, all other nodes in the area monitor the environment by reflected signals from objectives. By analyzing the propagation delay and the time scaling factor (i.e., the Doppler effect) of the reflected acoustic wave from the object [12], position and velocity information of the target can be estimated by jointly considering the observations from different nodes. The localization results are reported to onshore base station or control center through surface nodes, such as ships or buoys. Compared with conventional localization system

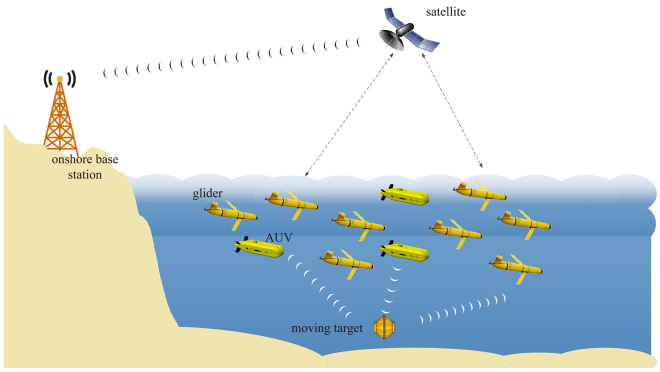

Fig. 1. An example of a mobile underwater acoustic array network.

relying on the larger number of fixed anchors, AUVs in the active mobile sonar system bring a lot of advantages such as low localization cost and wide coverage [13]. However, some challenging issues have to be carefully addressed, including synchronization, collaboration, speed differences among AUVs, and stratification effect on the sound speed in seawater.

In this paper, we employ a mobile underwater acoustic array network that consists of a swarm of AUVs or gliders, to locate the moving target. AUV relies on the inertial navigation system to track itself when diving. The accumulated positioning error and the clock drift are corrected by periodically surfacing to receive the GPS signals. We assume that one AUV periodically transmits linear frequency modulated (LFM) signals. The position and the velocity of the mobile target can be estimated by jointly considering the propagation delay and the Doppler factor measured by other nodes (i.e., other AUVs). The propagation delay and the Doppler factor are extracted from the received LFM signals reflected by the moving target. The main contributions of this paper are summarized as follows.

- Compared with fixed underwater acoustic array networks, we exploit the mobile underwater acoustic array network to locate the moving target to improve the scalability and feasibility of underwater localization. Moreover, there is no requirement of uniform velocities for all nodes (i.e., AUVs).
- We employ the Doppler factor and the propagation delay of acoustic signals, as two measurements, to jointly estimate the position and velocity of the moving target. Furthermore, we study the optimal weight matrix to evaluate different measurement errors of the Doppler factor and the propagation delay without any priori information.
- In the proposed localization algorithm, the sound speed is treated as an unknown variable. Moreover, we provide a low computational complexity initial estimation for the position and velocity of the moving target, which enables the estimation results to converge in two iterations.

The rest of this paper is organized as follows. We summarize the current work related with underwater localization in Section II. In Section III, we propose the system model of localization. Moreover, based on the proposed model, we establish the observation equations and design a refined iteration algorithm to improve the localization accuracy after a coarse initial estimation. In Section IV, we analyze the position and the velocity errors of the proposed algorithm and discuss the corresponding CRLB. We verify the proposed localization algorithm by simulations in Section V and conclude the paper in Section VI.

Notations: in this paper, the bold letters represent vectors or matrices. $\mathbb{E}\{\cdot\}$ is the expectation of a variable or a mathematical expression. Superscript T denotes the transpose of a matrix. $\|\cdot\|$ is the L_2 norm of a vector. $\{\hat{\cdot}\}$ and $\{\bar{\cdot}\}$ are the estimated and the average values of a variable or a mathematical expression, respectively.

II. Related Work

A. Framework of AUV-Aided Underwater Localization

AUVs rely on the two-way packet exchange to achieve time synchronization, which may bring high cost due to the limited bandwidth of underwater acoustic signals [11], [14], [15]. An alternative approach is to enable the AUVs periodically surface to synchronize and to locate themselves through the onboard GPS equipment [16]. By doing so, the time synchronization accuracy is at the level of $10\,\mathrm{ns}$, which is negligible for underwater acoustic communications and localization, because the acoustic signal significantly propagates much slower than electromagnetic waves. For the collaboration among AUVs, all AUVs are constantly detecting the reflected signals and all collected data must be aggregated for target's localization [9]. These operations may be constrained by the limited bandwidth of acoustic signals. One possible solution is that the AUVs only share the useful information (e.g., the estimated propagation delay and the Doppler rate) with others. Furthermore, the velocity differences among AUVs also affect the localization performance. The AUVs can estimate the real-time location and velocity of themselves through the onboard inertial sensors and then share these information with others. The shared information can be used for target location and velocity estimation. The basic idea is that the velocities of AUVs are assumed to be constant during a short duration (e.g., several seconds) for accurately modeling their effects during acoustic signal propagation.

B. Localization Using ToA and TDoA

We also realize that the time of arrival (ToA), the time differences of arrival (TDoA) are two typical measurements used in the localization system due to their small timing error [17]. In [18], a sequential time synchronization and localization algorithm is proposed to iteratively refine the localization accuracy by ToA reported from different locations. To improve the computational efficiency, the authors in [19] introduce a two-phase algorithm by jointly considering the time synchronization and localization. The tiny clock skew is ignored in the first phase and the coarse positioning estimation error is refined by least squares estimator in the second phase. Moreover, with consideration of the spatial-temporal correlation of underwater targets, the authors in [20] firstly propose an asynchronous intergradation localization solution for underwater localization including AUVs, active sensor nodes, and passive sensor nodes.

The AUVs establish the connection with the active sensor nodes via signaling exchange without explicit clock synchronization. The passive sensor nodes can establish the relationship between propagation delay and position information by listening to signaling exchange between AUVs and the active sensor nodes. However, the stratification effect in seawater causes the variation of underwater acoustic speed [21]. Therefore, it is difficult to accurately estimate the transmitter-receiver distance based on propagation delay by directly using the ToA and the TDoA in the marine environment. Two possible solutions can be considered. One is to accurately model the propagation of the acoustic signal by considering the stratification effect, by doing which we can improve ranging accuracy [22]. However, this leads to high computational complexity, and thus may not be friendly to real-time applications. Another solution is to view the average underwater sound speed as an extra unknown that can be estimated together with the target position. It has been shown that the second solution significantly reduces the computational complexity with negligible performance loss [7], [8], [23].

C. Doppler Effect Based Localization Algorithms

Compared with ToA and TDoA, the Doppler factor is another measurement that can be adopted in aquatic environment due to the slow sound speed in seawater compared with electromagnetic signal propagation in the air [24]. It relaxes the constraints of the time synchronization and the limited bandwidth of underwater acoustic signals. In [25], the authors exclusively employ the Doppler factor to estimate the position and velocity of the moving target. The target can conduct the localization process relying on the Doppler shift estimation of the sinusoid waves periodically transmitted by the AUV. Similarly, the Doppler shift estimation is utilized to locate moving targets by the static underwater acoustic array network [26].

On the other hand, the Doppler factor can be extracted from linear frequency modulated (LFM) and hyperbolic frequency modulated signals that are the typical probe signals widely used in the continuous active sonar system (CAS) [7]. It is known that traditional pulsed active sonar (PAS) systems employ frequency-modulated (FM) chirps to detect objects, which lead to the low detection probability due to the longer pulse repetition interval between any two transmissions [27]. The CAS system is believed to bring significant advantages in terms of the high success rate of target detection and the low false alarm rate [28], [29]. Based on the experimental results, the CAS system can effectively suppress the multi-path interference [28], [30]. The reason is that the phases of multi-path reflections are not stable, which can be averaged out during the signal process in the CAS system. Therefore, leveraging the balance between time and frequency domain resolutions, LFM signals are widely employed to ranging, localization, and tracking. Due to its time-variant signal spectrum, the Fractional Fourier transform (FrFT) is adopted to maintain low computational complexity in real-time applications [31]. In [26], [32], the propagation delay and the Doppler factor are obtained from the spectrum of the received LFM signals, which are used to jointly estimate the position and velocity of the targets. The combination of different types of measurements to estimate the target's position can be found in [33].

III. Localization With Mobile Underwater Acoustic Array Networks

In this section, we present the system model for underwater localization using mobile underwater acoustic array networks. Then, based on the system model, we propose the coarse estimation and the refinement algorithm for localization.

A. System Model

As shown in Fig. 1, we deploy $M+1$ acoustic nodes (e.g., AUVs or gliders), where node 0 periodically emits LFM signals to the moving target and the rest of nodes receive the signals reflected by the moving target. Assume that each node i in the mobile underwater acoustic array network and the moving target are moving at a constant speed of $\mathbf{v}_i = [v_{i,x}, v_{i,y}]^T$ and $\mathbf{v} = [v_x, v_y]^T$, respectively. Let τ_0 be the time duration of the LFM signal first reaching the moving target after emitted by node 0. Moreover, we assume that v_0 is the radial velocity of the moving target with respect to node 0. Similarly, v_i is the radial velocity of the moving target with respect to node i. Considering the mobility of the underwater acoustic array network and the moving target, the Doppler factor of node i, denoted by ρ_i, can be calculated by

$$\rho_i = \frac{c - v_0}{c + v_i}, \tag{1}$$

where c is the sound speed in the seawater. We can calculate v_0 and v_i as follows.

$$v_0 = \frac{(\mathbf{v}_0 - \mathbf{v})^T (\mathbf{x}_0 - \mathbf{x})}{\|\mathbf{x}_0 - \mathbf{x}\|}, \tag{2}$$

$$v_i = \frac{(\mathbf{v}_i - \mathbf{v})^T (\mathbf{x}_i - \mathbf{x})}{\|\mathbf{x}_i - \mathbf{x}\|}. \tag{3}$$

(2) and (3) are derived in Appendix A.

Moreover, let $\mathbf{x}_i = [x_{i,x}, x_{i,y}]^T$ and $\mathbf{x} = [x_x, x_y]^T$ denote the positions of node i and the moving target at $t = 0$, respectively. As discussed in Section II, the position and the velocity of node i, i.e., $\mathbf{v}_i, \mathbf{x}_i, i = 0, 1, \ldots M$ are assumed to be priori, which can be obtained by the inertial navigation system (INS) and GPS equipped on the AUV or glider [10], [11]. Let τ_0 be the time duration of the LFM signal omitted by node 0 to first arriving at the moving target. Then, we have $\tau_0 = \|\mathbf{x}_0 - \mathbf{x}\|/(c - v_0)$ and the position of the moving target at τ_0 is $\mathbf{x}_{\tau_0}$, which is calculated by $\mathbf{x}_{\tau_0} = \mathbf{x} + \mathbf{v}\tau_0$ (assume that v_0 is constant during τ_0). Let τ_i be the propagation delay of the reflected signal received by the i-th listening node. For a given receiving node i in the mobile underwater acoustic array network, we have

$$\|\mathbf{x}_0 - \mathbf{x}_{\tau_0}\| + \|\mathbf{x}_i + \mathbf{v}_i\tau_i - \mathbf{x}_{\tau_0}\| = c\tau_i. \tag{4}$$

In (4), it is worth noting that node i keeps moving during the propagation of the LFM signal. Thus, the distance between the moving target and node i before receiving the LFM signal reflected by the moving target is $\|\mathbf{x}_i + \mathbf{v}_i\tau_i - \mathbf{x}_{\tau_0}\|$.

Now, we establish the observation equations based on the Doppler factor and the propagation delay as shown in (1) and (4), respectively. Moreover, the Doppler factor and the propagation delay can be extracted from the received signals, which is discussed in the next section.

B. Signal Processing

Let $s(t)$ denote the LFM signal transmitted by a sending node in the underwater acoustic array network during $t \in [0, T]$, which can be expressed as

$$s(t) = Ae^{j(2\pi f_0 t + k\pi t^2)}. \tag{5}$$

In (5), A is the amplitude of the LFM signal, f_0 is the carrier frequency and k is the frequency rate. The corresponding received signal, reflected by the target and presented as another LFM signal, can be calculated by

$$r(t) = A_1 e^{j\left(2\pi f_0 \rho(t-\tau) + k\pi(\rho(t-\tau))^2\right)}, \tag{6}$$

where A_1, ρ, and τ are the amplitude of the received signal with propagation loss, the Doppler rate, and time delay of the received signal, respectively. We realize that each node can receive reflected signals from multiple paths due to the nature of the underwater acoustic channel. The noise can be assumed to be the additive Gaussian noise when the narrow-band acoustic system is adopted [34]. On the other hand, the moving target is expected to be discovered several kilometers away and the AUV is moving at the speed of several meters per seconds. This means that the Doppler factor can be assumed to be invariant during a few seconds because the radial distance between the AUV and the moving target in this short duration is much less than the distance between the AUV and the target. It has been proved that the strength of the multi-path interference can be decreased by increasing the number of samples [35]. In this case, we consider the received signal from the light-of-sight path that contains sufficient information for position and velocity estimation and other paths are treated as the interference [34].

After frequency mixing and low-pass filter processing, the resulting signal is

$$r(t) = A_2 e^{j\left(2\pi(f_0(1-\rho)+k\rho^2\tau)t + k\pi(1-\rho^2)t^2 + \zeta\right)}, \tag{7}$$

where A_2 is the amplitude of the signal after filtering and ζ is the phase delay of no significance for the localization purpose.

Let $\tilde{f}$ and $\tilde{k}$ be the parameters of the new LFM signal, i.e., the new carrier frequency and the new frequency rate, respectively. Compared (6) and (7), we have

$$\tilde{f} = f_0(1-\rho) + k\rho^2\tau, \text{and } \tilde{k} = k(1-\rho^2). \tag{8}$$

Then, (7) is rewritten as a standard form,

$$r(t) = \tilde{A}_2 e^{j\left(2\pi \tilde{f} t + \tilde{k}\pi t^2\right)}, \tag{9}$$

where $\tilde{A}_2 = A_2 e^{j\zeta}$ and $t \in [\tau_{\max}, T]$. $\tau_{\max}$ is the maximum propagation delay of the acoustic signals between the sender and a receiver.

As shown in (8), the values of τ and ρ rely on the $\tilde{f}$ and $\tilde{k}$. As the two parameters of the LFM signal, $\tilde{f}$ and $\tilde{k}$ can be obtained from the corresponding signal spectrum. Let an arbitrary received LFM signal with additive Gaussian noise (i.e., $n(t)$) be

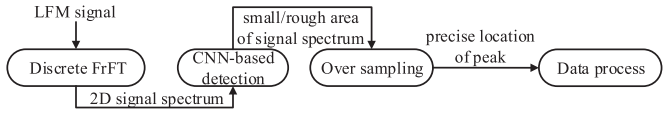

Fig. 2. Main process of the proposed algorithm.

$$\tilde{r}(t) = \tilde{A}_2 e^{j\left(2\pi f_0 t + k\pi t^2\right)} + n(t), t \in [0, T]. \tag{10}$$

The maximum likelihood estimation of the amplitude, the carrier frequency, and the frequency rate of the received LFM signal has been proved [26] to be reduced to

$$\left[\hat{f}_0, \hat{k}\right] = \arg\max_{\bar{f}_0, \bar{k}} \left| \int_{t=0}^{T} \tilde{r}(t) e^{-j(2\pi \bar{f}_0 t + \bar{k}\pi t^2)} dt \right|. \tag{11}$$

The values of $\hat{f}_0$ and $\hat{k}$ corresponding to the peaks can be obtained by two-dimensional (2D) search in the energy distribution of $\tilde{r}(t)$ after taking the Wigner distribution function of $\tilde{r}(t)$. However, this process results in high computational complexity even though it brings highest possible temporal and frequency resolutions compared with short-time Fourier transform. Therefore, we use the FrFT to process the received LFM signal, which is same as discussed in [30]. We briefly present the signal process with FrFT here. The a-th order FrFT of $\tilde{r}(t)$ is expressed as $R_a(u) = \int_{-\infty}^{\infty} K_a(u,t)\tilde{r}(t)dt$, where $K_a(u,t)$ is the kernel function calculated as

$$K_a(u,t) = \sqrt{1 - j\cot\phi} e^{j\pi(u^2\cot\phi - 2ut\csc\phi + t^2\cot\phi)}, \tag{12}$$

where $\phi = a\pi/2$. By taking two important properties of FrFT, i.e., $R_a(u) = R_{a+4}(u)$ and $R_a(u) = R_{a+2}(-u)$, the FrFT of the received LFM signal should be conducted for $a \in [-1, 1]$. Actually, the received LFM signal is decomposed into a series of LFM signals with respect to a and u that can form a 2D signal spectrum. Consequently, searching the maximum values of $\hat{f}_0$ and $\hat{k}$ is converted to searching the peak in the 2D signal spectrum $R_a(u)$. The maximum value of $R_a(u)$ can be achieved when

$$\hat{f}_0 = \hat{u}\csc\hat{\phi}, \text{ and } \hat{k} = -\cot\hat{\phi}, \tag{13}$$

where $\hat{\phi} = \hat{a}\pi/2$.

We also realize that directly using the FrFT to obtain the spectrum may not be realistic due to its high computational complexity in searching a large space. It is worth noting that the convolutional neural network (CNN) is adopted to identify the peaks of signals (i.e., corresponding existence of the moving target) in the spectrum [26]. Specifically, the CNN in the signal processing is able to output the rough area around the peak with low error rate after enough training. Then, over-sampling in the rough area of the spectrum is conducted to precisely capture the position of the peak. However, this part is out of scope of this paper. Here, we summarize the entire process of the proposed localization process in Fig. 2.

According to (8) and (13), we can obtain the values of the Doppler rate and the delay (i.e., ρ and τ). On the other hand, according to the localization system model powered by the

underwater acoustic array network, the mathematical relationships among the delay, the Doppler factor, the velocity, and the position of the moving target can be established. Furthermore, inspired by the best linear unbiased estimator (BLUE), the velocity and the position of the moving target can be jointly estimated by the delay and the Doppler factor, which is discussed in Section III-C.

C. Estimation Algorithm for Underwater Localization

As discussed in Section III-A, there are M nodes acting as receivers that can provide $2\,M$ observation equations. Specifically, node i generates two observation equations related to τ_i and ρ_i, respectively. Let $\boldsymbol{\beta}$ denote the vector of unknown parameters, which can be expressed as $\boldsymbol{\beta} = [\mathbf{x}_{\tau_0}^T, c, \mathbf{v}^T]^T$ and we have $2\,M$ equations with five unknown parameters. According to (1) and (4), the observation equations are nonlinear. In the case, we first derive the coarse result of $\boldsymbol{\beta}$ and then employ iterative algorithm, i.e., the Newton's method, to refine the result.

Let $d_0 = \|\mathbf{x}_0 - \mathbf{x}_{\tau_0}\|$ and rewrite (4) as

$$\|\mathbf{x}_i + \mathbf{v}_i\tau_i - \mathbf{x}_{\tau_0}\| = c\tau_i - d_0. \tag{14}$$

Squaring both sides of (14) and we have M equations as shown as follows,

$$\begin{aligned}&\|\mathbf{x}_i + \mathbf{v}_i\tau_i\|^2 + \|\mathbf{x}_{\tau_0}\|^2 - 2\mathbf{x}_{\tau_0}^T(\mathbf{x}_i + \mathbf{v}_i\tau_i)\\ &\quad = c^2\tau_i^2 - 2c\tau_i d_0 + d_0^2.\end{aligned} \tag{15}$$

We use the 2nd$\sim m$-th equations of (15) to minus the first equation of (15) to separate unknown parameters, respectively, which yields

$$\begin{aligned}&2(\mathbf{x}_1 + \mathbf{v}_1\tau_1)^T\mathbf{x}_{\tau_0} - 2(\mathbf{x}_i + \mathbf{v}_i\tau_i)^T\mathbf{x}_{\tau_0} - c^2\left(\tau_i^2 - \tau_1^2\right)\\ &\quad + 2cd_0(\tau_i - \tau_1) = -\|\mathbf{x}_i + \mathbf{v}_i\tau_i\|^2 + \|\mathbf{x}_1 + \mathbf{v}_1\tau_1\|^2,\end{aligned} \tag{16}$$

where $i \in \{2, 3, \ldots, M\}$. Suppose the current unknown parameter vector is $\boldsymbol{\theta} = [\mathbf{x}_{\tau_0}^T, c^2, cd_0]^T$, we establish the equation set as

$$\mathbf{B}\boldsymbol{\theta} = \mathbf{b}, \tag{17}$$

where $\mathbf{B}$ and $\mathbf{b}$ are shown at the bottom of this page. (17) can be solved by the least squares as $\boldsymbol{\theta} = (\mathbf{B}^T\mathbf{B})^{-1}\mathbf{B}^T\mathbf{b}$, which means that we are able to obtain the coarse values of $\mathbf{x}_{\tau_0}$ and c. Now we rewrite (1) as given in (18), shown at the bottom of this page.

$$\begin{aligned}c(\rho_i - 1) &= \rho_i\frac{\mathbf{v}^T(\mathbf{x}_i - \mathbf{x}_{\tau_0})}{\|\mathbf{x}_i - \mathbf{x}_{\tau_0}\|} + \frac{\mathbf{v}^T(\mathbf{x}_0 - \mathbf{x}_{\tau_0})}{\|\mathbf{x}_0 - \mathbf{x}_{\tau_0}\|}\\ &\quad - \rho_i\frac{\mathbf{v}_i^T(\mathbf{x}_i - \mathbf{x}_{\tau_0})}{\|\mathbf{x}_i - \mathbf{x}_{\tau_0}\|} - \frac{\mathbf{v}_0^T(\mathbf{x}_0 - \mathbf{x}_{\tau_0})}{\|\mathbf{x}_0 - \mathbf{x}_{\tau_0}\|}.\end{aligned} \tag{19}$$

Similarly, we use 2nd$\sim M$-th equations of (19) to minus the first equation of (19) to separate unknown parameters, respectively and we have

$$\begin{aligned}c(\rho_i - \rho_1) &= \rho_i\frac{\mathbf{v}^T(\mathbf{x}_i - \mathbf{x}_{\tau_0})}{\|\mathbf{x}_i - \mathbf{x}_{\tau_0}\|} - \rho_1\frac{\mathbf{v}^T(\mathbf{x}_1 - \mathbf{x}_{\tau_0})}{\|\mathbf{x}_1 - \mathbf{x}_{\tau_0}\|}\\ &\quad - \rho_i\frac{\mathbf{v}_i^T(\mathbf{x}_i - \mathbf{x}_{\tau_0})}{\|\mathbf{x}_i - \mathbf{x}_{\tau_0}\|} + \rho_1\frac{\mathbf{v}_1^T(\mathbf{x}_1 - \mathbf{x}_{\tau_0})}{\|\mathbf{x}_1 - \mathbf{x}_{\tau_0}\|}.\end{aligned} \tag{20}$$

Reorganize $M - 1$ equations like (20), we have

$$\mathbf{D}\mathbf{v} = \mathbf{d}, \tag{21}$$

where

$$\mathbf{D} = \begin{bmatrix}\frac{\rho_2(\mathbf{x}_2 - \mathbf{x}_{\tau_0})^T}{\|\mathbf{x}_2 - \mathbf{x}_{\tau_0}\|} - \frac{\rho_1(\mathbf{x}_1 - \mathbf{x}_{\tau_0})^T}{\|\mathbf{x}_1 - \mathbf{x}_{\tau_0}\|}\\ \vdots\\ \frac{\rho_M(\mathbf{x}_M - \mathbf{x}_{\tau_0})^T}{\|\mathbf{x}_M - \mathbf{x}_{\tau_0}\|} - \frac{\rho_1(\mathbf{x}_1 - \mathbf{x}_{\tau_0})^T}{\|\mathbf{x}_1 - \mathbf{x}_{\tau_0}\|}\end{bmatrix},$$

$$\mathbf{d} = \begin{bmatrix}\frac{\rho_2\mathbf{v}_2^T(\mathbf{x}_2 - \mathbf{x}_{\tau_0})}{\|\mathbf{x}_2 - \mathbf{x}_{\tau_0}\|} - \frac{\rho_1\mathbf{v}_1^T(\mathbf{x}_1 - \mathbf{x}_{\tau_0})}{\|\mathbf{x}_1 - \mathbf{x}_{\tau_0}\|} + c(\rho_2 - \rho_1)\\ \vdots\\ \frac{\rho_M\mathbf{v}_M^T(\mathbf{x}_M - \mathbf{x}_{\tau_0})}{\|\mathbf{x}_M - \mathbf{x}_{\tau_0}\|} - \frac{\rho_1\mathbf{v}_1^T(\mathbf{x}_1 - \mathbf{x}_{\tau_0})}{\|\mathbf{x}_1 - \mathbf{x}_{\tau_0}\|} + c(\rho_M - \rho_1)\end{bmatrix}. \tag{22}$$

In practice, it is difficult to obtain the true values of τ_i and ρ_i. Therefore, we utilize the measurement values of τ_i and ρ_i that are the outputs of node i (i.e., $\hat{\tau}_i$ and $\hat{\rho}_i$) in the above equations to estimate the unknown parameters in $\boldsymbol{\beta}$. By using the coarse results from (17), we can derive the coarse value of $\mathbf{v}$. So far, we have the initial values of the unknown parameters, denoted by $\boldsymbol{\beta}^{(0)}$, which is used in the following part to refine results.

The partial derivatives of (1) and (4) may not be directly derived because the observation variables can not be completely separated. Thus, we reorganize (1) and (4) as follows. The objective of the deployed underwater acoustic array network is to detect the moving target beyond a long distance, e.g., tens of kilometers. On the other hand, the AUV/glider can cruise at

$$\mathbf{B} = \begin{bmatrix}2(\mathbf{x}_1 + \mathbf{v}_1\tau_1)^T - 2(\mathbf{x}_2 + \mathbf{v}_2\tau_2)^T & -\left(\tau_2^2 - \tau_1^2\right) & 2(\tau_2 - \tau_1)\\ \vdots & \vdots & \vdots\\ 2(\mathbf{x}_1 + \mathbf{v}_1\tau_1)^T - 2(\mathbf{x}_M + \mathbf{v}_M\tau_M)^T & -\left(\tau_M^2 - \tau_1^2\right) & 2(\tau_M - \tau_1)\end{bmatrix},$$

$$\mathbf{b} = \begin{bmatrix}\|\mathbf{x}_1 + \mathbf{v}_1\tau_1\|^2 - \|\mathbf{x}_2 + \mathbf{v}_2\tau_2\|^2\\ \vdots\\ \|\mathbf{x}_1 + \mathbf{v}_1\tau_1\|^2 - \|\mathbf{x}_M + \mathbf{v}_M\tau_M\|^2\end{bmatrix}. \tag{18}$$

several knots or several tens of knots. One knot is approximately $0.514\,\mathrm{m/s}$. The delay of the received LFM signal is around one or several seconds. In this case, we have $\|\mathbf{v}_i\tau_i\| \ll \|\mathbf{x}_i - \mathbf{x}_{\tau_0}\|$ and (4) is rewritten as

$$\tau_i \approx \frac{\|\mathbf{x}_0 - \mathbf{x}_{\tau_0}\| + \|\mathbf{x}_i - \mathbf{x}_{\tau_0}\|}{c} = g_{\tau_i}(\boldsymbol{\beta}). \tag{23}$$

As $v_0/c \ll 1$ and $v_i/c \ll 1$, we rewrite (1) by taking the first order Taylor expansion as

$$\rho_i = \frac{c - v_0}{c + v_i} \approx 1 - \frac{1}{c}(v_0 + v_i) = g_{\rho_i}(\boldsymbol{\beta}). \tag{24}$$

Then, combining (23) and (24), we establish the observation equation set as

$$\mathbf{g}(\boldsymbol{\beta}) = [g_{\tau_1}(\boldsymbol{\beta}), \ldots, g_{\tau_M}(\boldsymbol{\beta}), g_{\rho_1}(\boldsymbol{\beta}), \ldots, g_{\rho_M}(\boldsymbol{\beta})]^T, \tag{25}$$

and the corresponding observation vector is

$$\boldsymbol{\gamma} = [\hat{\tau}_1, \ldots, \hat{\tau}_M, \hat{\rho}_1, \ldots, \hat{\rho}_M]^T. \tag{26}$$

Converting the observation equation set to the corresponding matrix set, we have

$$\mathbf{g}(\boldsymbol{\beta}) = \boldsymbol{\gamma}. \tag{27}$$

Let $\Delta\boldsymbol{\beta} = \boldsymbol{\beta}^{(0)} - \boldsymbol{\beta}$ be the estimation error of $\boldsymbol{\beta}$ and

$$\nabla\mathbf{g} = \left[\frac{\partial g_{\tau_1}(\boldsymbol{\beta})}{\partial\boldsymbol{\beta}}, \ldots, \frac{\partial g_{\tau_M}(\boldsymbol{\beta})}{\partial\boldsymbol{\beta}}, \frac{\partial g_{\rho_1}(\boldsymbol{\beta})}{\partial\boldsymbol{\beta}}, \ldots, \frac{\partial g_{\rho_M}(\boldsymbol{\beta})}{\partial\boldsymbol{\beta}}\right]^T, \tag{28}$$

where each element is presented in Appendix B.

Each node in the underwater acoustic array network independently observes the delay and Doppler factor that are represented in (1) and (4). It is realistic that the variances of all observations may not be equal. Therefore, $\Delta\boldsymbol{\beta}$ can be calculated by BLUE as shown as follow,

$$\Delta\boldsymbol{\beta} = \left(\mathbf{G}(\boldsymbol{\beta})^T\mathbf{W}\mathbf{G}(\boldsymbol{\beta})\right)^{-1}\mathbf{G}(\boldsymbol{\beta})^T\mathbf{W}\left(\mathbf{g}(\boldsymbol{\beta}) - \boldsymbol{\gamma}\right), \tag{29}$$

where $\mathbf{G}(\boldsymbol{\beta}) = \nabla\mathbf{g}$. In practice, $\mathbf{G}(\boldsymbol{\beta}^{(n)}) = \nabla\mathbf{g}\big|_{\boldsymbol{\beta}=\boldsymbol{\beta}^{(n)}}$ is used to calculate because $\boldsymbol{\beta}$ is unknown, where $\boldsymbol{\beta}^{(n)}$ is the estimation value of $\boldsymbol{\beta}$ in n-th iteration. For example, at the initial step (i.e., $n = 0$), $\mathbf{G}(\boldsymbol{\beta}^{(0)}) = \nabla\mathbf{g}\big|_{\boldsymbol{\beta}=\boldsymbol{\beta}^{(0)}}$. Then, $\boldsymbol{\beta}$ can be updated by $\boldsymbol{\beta}^{(1)} = \boldsymbol{\beta}^{(0)} + \Delta\boldsymbol{\beta}$. $\mathbf{W}$ is the weight matrix that presents the relationship among $\hat{\tau}_i$ and $\hat{\rho}_i$. However, it is difficult to clearly quantify $\sigma^2_{\tau_i}$ and $\sigma^2_{\rho_i}$ without any prior information for estimation. In this case, we prove that the optimal weight matrix $\mathbf{W}$ should be inverse of the covariance matrix of observations, which is presented in Appendix C.

Algorithm 1 describes the detail of the Newton's method incorporated with BLUE, where ε and N represent the required estimation accuracy and the number of iterations, respectively. In Algorithm 1, the final estimation results are converged in few number of iterations, which are reported in Section V. The main computational complexity of Newton's method results from the matrix inversion and the computational complexity is $\mathcal{O}(n^3)$.

Algorithm 1: Newton's Method Using BLUE.

Require: $\boldsymbol{\gamma}$ (measurement delay and the Doppler factor)
Ensure: $\hat{\boldsymbol{\beta}}$ (the location and velocity estimation of the moving target and sound speed estimation)
1: Initialization: $\boldsymbol{\beta}^{(0)}$, ε, N, $n = 1$; $\boldsymbol{\beta}^{(1)} = \boldsymbol{\beta}^{(0)}$;
2: **while** $n < N$ and $\|\Delta\boldsymbol{\gamma}\| > \varepsilon$ **do**
3: $\quad\Delta\boldsymbol{\gamma} = \mathbf{g}(\boldsymbol{\beta}^{(n)}) - \boldsymbol{\gamma}$;
4: $\quad\Delta\boldsymbol{\beta} = (\mathbf{G}(\boldsymbol{\beta}^{(n)})^T\mathbf{W}\mathbf{G}(\boldsymbol{\beta}^{(n)}))^{-1}\mathbf{G}(\boldsymbol{\beta}^{(n)})^T\mathbf{W}\Delta\boldsymbol{\gamma}$;
5: $\quad\boldsymbol{\beta}^{(n+1)} = \boldsymbol{\beta}^{(n)} + \Delta\boldsymbol{\beta}$;
6: $\quad n = n + 1$
7: **end while**

IV. Positioning and Velocity Errors Analysis

A. Error Analysis of the Proposed Algorithm

The errors of position and velocity are inevitable due to the measurement errors of the Doppler factor and the delay, which result from the measurement errors of $\hat{a}$ and $\hat{u}$ observed from the 2D spectrum of the received LFM signal as discussed in Section III-A. It is realistic to assume that the measurement errors on different nodes are independent and identically distributed (i.i.d.). Thus, we have $\Delta\boldsymbol{\beta} = (\mathbf{G}(\boldsymbol{\beta}^{(n)})^T\mathbf{W}\mathbf{G}(\boldsymbol{\beta}^{(n)}))^{-1}\mathbf{G}(\boldsymbol{\beta}^{(n)})^T\mathbf{W}\boldsymbol{\varepsilon}_{\boldsymbol{g}(\boldsymbol{\beta})}$, where $\boldsymbol{\varepsilon}_{\boldsymbol{g}(\boldsymbol{\beta})}$ is the estimation error of $\boldsymbol{\gamma}$. Then, we calculate the covariance matrix of $\hat{\boldsymbol{\beta}}$ as shown in (30).

$$\begin{aligned}\mathrm{cov}(\hat{\boldsymbol{\beta}}, \hat{\boldsymbol{\beta}}) &= \mathbb{E}\left\{(\hat{\boldsymbol{\beta}} - \boldsymbol{\beta})(\hat{\boldsymbol{\beta}} - \boldsymbol{\beta})^T\right\} \\ &= \mathbb{E}\left\{\left(\mathbf{G}(\boldsymbol{\beta})^T\mathbf{W}\mathbf{G}(\boldsymbol{\beta})\right)^{-1}\mathbf{G}(\boldsymbol{\beta})^T\mathbf{W}\boldsymbol{\varepsilon}_{\boldsymbol{g}(\boldsymbol{\beta})}\right. \\ &\quad\left.\cdot\left[\left(\mathbf{G}(\boldsymbol{\beta})^T\mathbf{W}\mathbf{G}(\boldsymbol{\beta})\right)^{-1}\mathbf{G}(\boldsymbol{\beta})^T\mathbf{W}\boldsymbol{\varepsilon}_{\boldsymbol{g}(\boldsymbol{\beta})}\right]^T\right\} \\ &\approx \left(\mathbf{G}(\boldsymbol{\beta})^T\mathbf{W}\mathbf{G}(\boldsymbol{\beta})\right)^{-1}.\end{aligned} \tag{30}$$

In (30), we implicitly adopt the conclusion in Appendix C, which presents the optimal weight matrix $\mathbf{W} = (\boldsymbol{\varepsilon}_{\boldsymbol{g}(\boldsymbol{\beta})}\boldsymbol{\varepsilon}^T_{\boldsymbol{g}(\boldsymbol{\beta})})^{-1}$ when the observations do not provide any prior information.

As discussed in (8) and (13), the relationship between (τ, ρ) and (a, u) is nonlinear. Considering Gaussian distribution exhibiting the highest uncertainty [36], [37], we assume that τ and ρ follow Gaussian distribution and discuss the CRLB of the proposed algorithm to evaluate the localization performance using the mobile underwater acoustic array network. Because the observation of each node is independent, we have $\mathrm{cov}(\hat{\tau}_i, \hat{\rho}_j) = 0, \mathrm{cov}(\hat{\tau}_i, \hat{\tau}_j) = 0, \mathrm{cov}(\hat{\rho}_i, \hat{\rho}_j) = 0$ when $i \neq j$. The probability density function of $\boldsymbol{\gamma}$ is

$$\begin{aligned}f(\boldsymbol{\gamma}|\boldsymbol{\beta}) &= \frac{1}{(2\pi)^{2M/2}|\boldsymbol{\Sigma}|^{1/2}} \\ &\quad\cdot\exp\left(-\frac{(\boldsymbol{\gamma} - \boldsymbol{\mu}_{\boldsymbol{\gamma}})^T\boldsymbol{\Sigma}^{-1}(\boldsymbol{\gamma} - \boldsymbol{\mu}_{\boldsymbol{\gamma}})}{2}\right),\end{aligned} \tag{31}$$

where $\boldsymbol{\mu}_{\boldsymbol{\gamma}}$ is the mean value of $\boldsymbol{\gamma}$. $\boldsymbol{\Sigma}$ is the covariance matrix of τ and ρ that can be expressed as follows,

$$\boldsymbol{\Sigma} = \begin{bmatrix} \boldsymbol{\Sigma}_{1,1} & \boldsymbol{\Sigma}_{1,2} \\ \boldsymbol{\Sigma}_{2,1} & \boldsymbol{\Sigma}_{2,2} \end{bmatrix}, \tag{32}$$

where

$$\begin{aligned} \boldsymbol{\Sigma}_{1,1} &= \operatorname{diag}\left\{[\sigma^2_{\tau_1}, \sigma^2_{\tau_2}, \ldots \sigma^2_{\tau_M}]\right\}, \\ \boldsymbol{\Sigma}_{1,2} &= \boldsymbol{\Sigma}_{2,1} = \operatorname{diag}\left\{[\operatorname{cov}(\tau_1, \rho_1), \ldots, \operatorname{cov}(\tau_M, \rho_M)]\right\}, \\ \boldsymbol{\Sigma}_{2,2} &= \operatorname{diag}\left\{[\sigma^2_{\rho_1}, \sigma^2_{\rho_2}, \ldots \sigma^2_{\rho_M}]\right\}. \end{aligned} \tag{33}$$

The logarithm of $f(\boldsymbol{\gamma}|\boldsymbol{\beta})$ can be presented as

$$\ln f(\boldsymbol{\gamma}|\boldsymbol{\beta}) = \ln\left(\frac{1}{(2\pi)^{2M/2}|\boldsymbol{\Sigma}|^{1/2}}\right) - \frac{(\boldsymbol{\gamma}-\boldsymbol{\mu}_{\boldsymbol{\gamma}})^T \boldsymbol{\Sigma}^{-1}(\boldsymbol{\gamma}-\boldsymbol{\mu}_{\boldsymbol{\gamma}})}{2}. \tag{34}$$

Then the Fisher information matrix is

$$\mathbf{F} = -\mathbb{E}\left\{\nabla^2_{\boldsymbol{\beta}}(\ln f)\right\}. \tag{35}$$

Therefore, we utilize the methods discussed in [25], [38] to derive the expression of each element in the Fisher information matrix, denoted by $\mathbf{F}[i,j]$, which is shown as follows,

$$\mathbf{F}[i,j] = \left(\frac{\partial \boldsymbol{\mu}_{\boldsymbol{\gamma}}}{\partial \boldsymbol{\beta}[i]}\right)^T \boldsymbol{\Sigma}^{-1} \frac{\partial \boldsymbol{\mu}_{\boldsymbol{\gamma}}}{\partial \boldsymbol{\beta}[j]} + \frac{1}{2}\operatorname{Tr}\left(\boldsymbol{\Sigma}^{-1}\frac{\partial \boldsymbol{\Sigma}}{\partial \boldsymbol{\beta}[i]}\boldsymbol{\Sigma}^{-1}\frac{\partial \boldsymbol{\Sigma}}{\partial \boldsymbol{\beta}[j]}\right). \tag{36}$$

The second term of (36) can be ignored. In Appendix D, a formal proof is presented to show that

$$\frac{1}{2}\operatorname{Tr}\left(\boldsymbol{\Sigma}^{-1}\frac{\partial \boldsymbol{\Sigma}}{\partial \boldsymbol{\beta}[i]}\boldsymbol{\Sigma}^{-1}\frac{\partial \boldsymbol{\Sigma}}{\partial \boldsymbol{\beta}[j]}\right) \approx 0. \tag{37}$$

Now, the Fisher information matrix can be expressed as

$$\mathbf{F} \approx \left(\frac{\partial \boldsymbol{\mu}_{\boldsymbol{\gamma}}}{\partial \boldsymbol{\beta}}\right)^T \boldsymbol{\Sigma}^{-1}\frac{\partial \boldsymbol{\mu}_{\boldsymbol{\gamma}}}{\partial \boldsymbol{\beta}}. \tag{38}$$

Let $\mathbf{H} = \frac{\partial \boldsymbol{\mu}_{\boldsymbol{\gamma}}}{\partial \boldsymbol{\beta}}$. In Appendix C, the optimal weight matrix is proved to be the inverse of the covariance matrix of observation variables. Thus, the Fisher information matrix can be rewritten as

$$\mathbf{F} \approx \mathbf{H}^T\mathbf{W}\mathbf{H}. \tag{39}$$

B. Covariance Matrix Calculation

As discussed in Section IV-A, the optimal weight matrix should be the inverse of the covariance matrix of observation variables. In (8) and (13), the relationship between (τ, ρ) and (a, u) is nonlinear. The quantization error caused by FrFT and the noise of the received signals dominate the observation errors of τ and ρ. It is difficult to obtain the covariance matrix of the observation variables in a closed-form fashion. In this paper, we use the empirical results to calculate the covariance matrix of τ and ρ. In general, we identify the value ranges of τ and ρ and evenly sample the values of τ and ρ in the corresponding ranges. The errors of each pair of τ_i and ρ_j $(1 \le i \le N$ and $1 \le j \le L)$ can be obtained via simulation for a certain signal-to-noise ratio (SNR) (i.e., $\mathrm{SNR}_k, 1 \le k \le K$). And then, the corresponding covariance of (τ_i, ρ_j) can be obtained. Based on the errors of τ_i and ρ_j as well as the corresponding covariance, we establish several two-dimension table indexed by τ and ρ for different SNRs. A table under SNR_k is shown in Table I. Each element in Table I is given by

TABLE I
A TABLE FOR COVARIANCE MATRIX CALCULATION

$\boldsymbol{\Sigma}_{\tau_1,\rho_1,k}$	$\boldsymbol{\Sigma}_{\tau_1,\rho_2,k}$	$\cdots$	$\boldsymbol{\Sigma}_{\tau_1,\rho_{L-1},k}$	$\boldsymbol{\Sigma}_{\tau_1,\rho_L,k}$
$\boldsymbol{\Sigma}_{\tau_2,\rho_1,k}$	$\boldsymbol{\Sigma}_{\tau_2,\rho_2,k}$	$\cdots$	$\boldsymbol{\Sigma}_{\tau_2,\rho_{L-1},k}$	$\boldsymbol{\Sigma}_{\tau_2,\rho_L,k}$
$\vdots$	$\vdots$	$\vdots$	$\vdots$	$\vdots$
$\vdots$	$\vdots$	$\vdots$	$\vdots$	$\vdots$
$\cdots$	$\cdots$	$\boldsymbol{\Sigma}_{\tau_{i-1},\rho_j,k}$	$\cdots$	$\cdots$
$\cdots$	$\boldsymbol{\Sigma}_{\tau_i,\rho_{j-1},k}$	$\boldsymbol{\Sigma}_{\tau_i,\rho_j,k}$	$\boldsymbol{\Sigma}_{\tau_i,\rho_{j+1},k}$	$\cdots$
$\vdots$	$\vdots$	$\boldsymbol{\Sigma}_{\tau_{i+1},\rho_j,k}$	$\vdots$	$\vdots$
$\cdots$	$\cdots$	$\cdots$	$\cdots$	$\cdots$
$\vdots$	$\vdots$	$\vdots$	$\vdots$	$\vdots$
$\boldsymbol{\Sigma}_{\tau_N,\rho_1,k}$	$\boldsymbol{\Sigma}_{\tau_N,\rho_2,k}$	$\cdots$	$\cdots$	$\boldsymbol{\Sigma}_{\tau_N,\rho_L,k}$

$$\boldsymbol{\Sigma}_{\tau_i,\rho_j,k} = \begin{bmatrix} \sigma^2_{\tau_i,k} & \operatorname{cov}_k(\tau_i,\rho_j) \\ \operatorname{cov}_k(\tau_i,\rho_j) & \sigma^2_{\rho_i,k} \end{bmatrix}. \tag{40}$$

We can obtain the table through off-line training. After establishing this table, the weight matrix $\mathbf{W}$ can be obtained by enquiring this table according to the measurement results of τ and ρ (i.e., the elements in $\boldsymbol{\gamma}$) when execute the proposed positioning algorithm. We also realize that the sampled values and measured values of τ and ρ may not be exactly equal. In this case, we use average values of the adjacent four matrixes of (τ, ρ), such as $\boldsymbol{\Sigma}_{\tau_{i-1},\rho_j}, \boldsymbol{\Sigma}_{\tau_i,\rho_{j-1}}, \boldsymbol{\Sigma}_{\tau_{i+1},\rho_j}, \boldsymbol{\Sigma}_{\tau_i,\rho_{j+1}}$.

V. PERFORMANCE EVALUATION

In this section, we conduct the simulation to evaluate the proposed localization algorithm with a mobile underwater acoustic array network. First, we demonstrate the simulation parameters. Then, we discuss the simulation results under different simulation parameters to verify the performance of the proposed localization algorithm.

A. Simulation Parameters

The initial frequency of the LFM signal is 1 kHz and the frequency rate is 50 Hz/s. The FrFT of the received signals is operated for the last 4 s to avoid ambiguity when the scanning period is configured as 8 s. We obtain the signal parameters as shown in (8) after the frequency mixing of the received and local probe signals. The sampling frequency, i.e. f_s, is at 400 Hz and the following operations including the zero-padding and the fast discrete FrFT. The mobile acoustic array network including nine nodes is deployed in the two dimensional coordination, where one node acts as the sender and the other are receiving nodes. In our simulation, the other nodes are located at $[0,0]^T$m, $[2000,2000]^T$m, $[2000,-2000]^T$m, $[-2000,2000]^T$m, $[-2000,-2000]^T$m, $[1000,1000]^T$m, $[1000,-1000]^T$m,

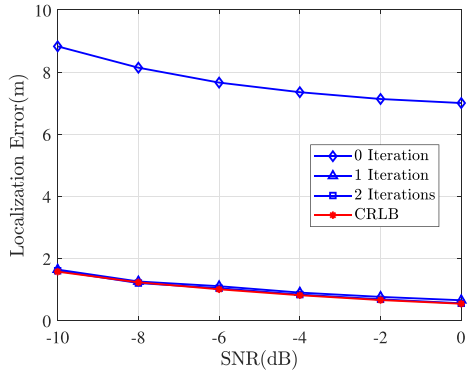

Fig. 3. Localization error with different number of iterations.

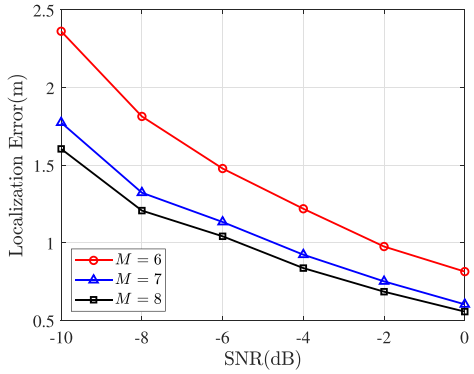

Fig. 5. Localization error with different numbers of nodes.

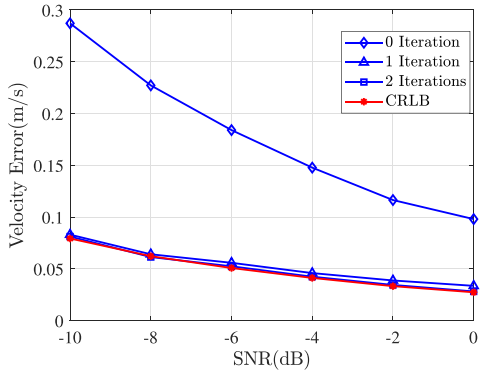

Fig. 4. Velocity error with different number of iterations.

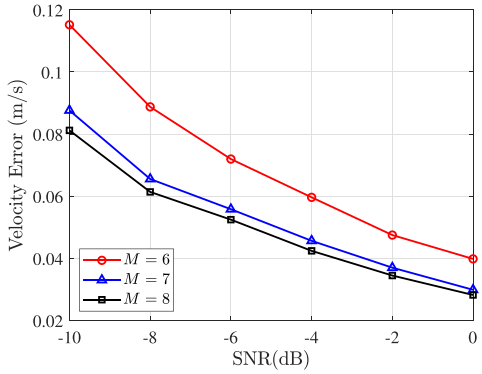

Fig. 6. Velocity error with different numbers of nodes.

$[-1000, 1000]^T\mathrm{m}$, $[-1000, -1000]^T\mathrm{m}$, respectively. The corresponding speeds are $[1, 1]^T\mathrm{m/s}$, $[1, 1]^T\mathrm{m/s}$, $[2, 2]^T\mathrm{m/s}$, $[3, 3]^T\mathrm{m/s}$, $[1, 3]^T\mathrm{m/s}$, $[1, 1]^T\mathrm{m/s}$, $[3, 1]^T\mathrm{m/s}$, $[2, 1]^T\mathrm{m/s}$, $[1, 2]^T\mathrm{m/s}$, respectively. The target is moving at speed of $[2, 1]^T\mathrm{m/s}$ with the initial location at $[0, 1500]^T\mathrm{m}$.

As mentioned in Section III-A, node 0 sends LFM signals and node i receives signals reflected by the moving target. To understand the distance between 0 and node i, these two nodes and the moving target can be served as two foci of an ellipse and any point on the ellipse, respectively. As the received signal processing for the last 4 s in our simulation, the maximum traveling distance of the LFM signal is around $6000\,\mathrm{m}$ ($4\,\mathrm{s} \times 1500\,\mathrm{m/s}$). Thus, the distance between node 0 and node i (i.e., the distance between two foci) should be shorter than $6000\,\mathrm{m}$. The size of the detection area increases when the distance between two foci decreases. On the other hand, the geometric dilution of precision (GDOP) of the proposed algorithm becomes worse when the distance between node 0 and node i decreases.

B. Localization and Velocity Estimation

We evaluate the localization and velocity errors of the proposed algorithm in terms of the SNR of the received signal and the number of iterations in Fig. 3 and Fig. 4, respectively. It is obvious that the estimation errors of localization and velocity decrease with the increase of the SNR. Furthermore, the estimation errors of localization and velocity errors are close to the CRLB after two iterations, which means that the performance of the proposed algorithm can achieve the optimal performance theoretically. The positioning error of the moving target is around $1.57\,\mathrm{m}$ when the SNR is $-10\,\mathrm{dB}$ and can be achieved at the level of $0.5\,\mathrm{m}$ when the SNR is $0\,\mathrm{dB}$. Similar improvement can be found in the velocity estimation of the moving target as shown in Fig. 4.

We also investigate the performance of the proposed localization algorithm with different number of nodes in the underwater acoustic array network. In Fig. 5 and Fig. 6, it is obvious that the positioning errors decrease by increasing the number of nodes. We also observe the similar trend in the velocity estimation. Moreover, with the increase of the SNR of the received signal, the estimation errors of the position and the velocity decrease with different number of nodes. To be specific, in a low SNR marine environment, when the number of the nodes in the mobile underwater acoustic array network increases from 6 to 8, the corresponding estimation accuracy of position approximately increases from $2.4\,\mathrm{m}$ to $1.57\,\mathrm{m}$. The corresponding estimation accuracy of velocity increases from $0.12\,\mathrm{m/s}$ to $0.08\,\mathrm{m/s}$. The similar trend of estimation accuracy improvement can also be observed in a high SNR environment.

We compare the proposed algorithm with the localization algorithm discussed in [26] in terms of absolute values of positioning and velocity errors and corresponding cumulative probability functions (CDF) under different SNRs. In [26], the observation equations are derived without considering the movement of nodes deployed in the underwater acoustic array network, which can be solved by the Newton's method with the

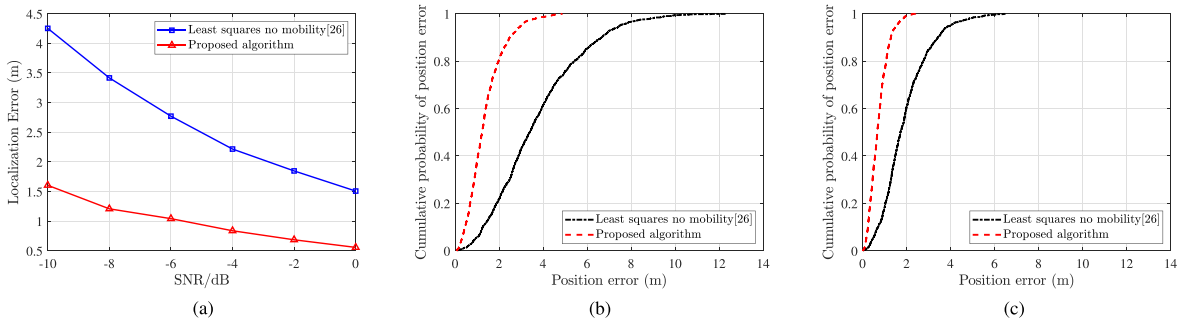

Fig. 7. Localization errors using different schemes: the localization algorithm without considering the mobility of underwater acoustic array networks and the proposed algorithm. (a) Numeric results. (b) CDF (SNR $= -10$ dB). (c) CDF (SNR $= 0$ dB).

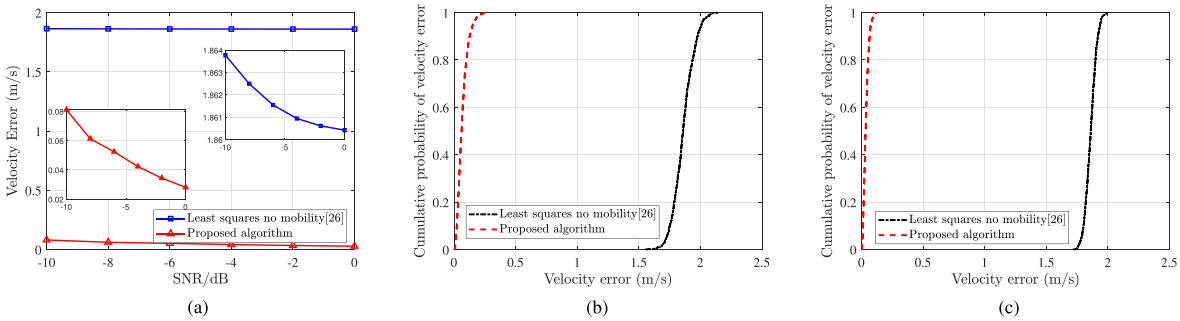

Fig. 8. Velocity errors using different schemes: the localization algorithm without considering the mobility of underwater acoustic array networks and the proposed algorithm. (a) Numeric results. (b) CDF (SNR $= -10$ dB). (c) CDF (SNR $= 0$ dB).

least squares. In Fig. 7 and Fig. 8, it is obvious that the proposed algorithm can achieve better performance compared with the algorithm in [26] in terms of localization error and velocity error. By taking the movement of nodes into consideration, the observation equations, i.e., (1) and (4), are solved by the proposed algorithm with BLUE. The localization accuracy can achieve the CRLB just two iterations as shown in Fig. 3 and Fig. 4, respectively.

VI. Conclusion

In this paper, we study a new approach for simultaneous target localization and velocity estimation using a mobile underwater acoustic array network. By utilizing the propagation delay and the Doppler effect extracted from the LFM signal, the proactive target localization and velocity estimation can outperform the baseline method utilizing the least squares. Specifically, we first establish the observation equations by analyzing the spectrum of the LFM signals and then utilize the Newton's method for target position and velocity estimation. To evaluate the localization and velocity estimation error, we derive the corresponding CRLBs for reference and comparison. Simulation results show that the system performance effectively approaches the bounds and a small array network is sufficient to achieve high accurate position and velocity estimation of underwater moving objects.

Appendix A
Derivation of v_0 and v_i

$\mathbf{x}_i$ and $\mathbf{x}$ are the positions of node i and the moving target at $t = 0$, respectively. Let d_i and Δd_i be the distances between node i and the moving target at the beginning and after t s, respectively, which are presented as

$$d_i = \|\mathbf{x}_i - \mathbf{x}\|, \tag{41}$$

$$\Delta d_i = \|\mathbf{x}_i - \mathbf{x} + (\mathbf{v}_i - \mathbf{v})t\|. \tag{42}$$

Therefore, we have

$$\begin{aligned} v_i &= \frac{\mathrm{d}(\Delta d_i)}{\mathrm{d}t} \\ &= \frac{(\mathbf{v}_i - \mathbf{v})^T(\mathbf{x}_i - \mathbf{x} + (\mathbf{v}_i - \mathbf{v})t)}{\|\mathbf{x}_i - \mathbf{x} + (\mathbf{v}_i - \mathbf{v})t\|}. \end{aligned} \tag{43}$$

Considering $d_i \gg \|(\mathbf{v} - \mathbf{v}_i)t\|$, (43) can be rewritten as

$$v_i \approx \frac{(\mathbf{v}_i - \mathbf{v})^T(\mathbf{x}_i - \mathbf{x})}{\|\mathbf{x}_i - \mathbf{x}\|}. \tag{44}$$

Appendix B
Each Element in (28)

All elements in (28) are shown as follows,

$$\begin{aligned} \frac{\partial g_{\tau_i}(\boldsymbol{\beta})}{\partial \mathbf{x}_{\tau_0}} &= -\frac{1}{c}\left(\frac{\mathbf{x}_0 - \hat{\mathbf{x}}_{\tau_0}}{\|\mathbf{x}_0 - \hat{\mathbf{x}}_{\tau_0}\|} + \frac{\mathbf{x}_i - \hat{\mathbf{x}}_{\tau_0}}{\|\mathbf{x}_i - \hat{\mathbf{x}}_{\tau_0}\|}\right), \\ \frac{\partial g_{\tau_i}(\boldsymbol{\beta})}{\partial c} &= -\frac{\|\mathbf{x}_0 - \hat{\mathbf{x}}_{\tau_0}\| + \|\mathbf{x}_i - \hat{\mathbf{x}}_{\tau_0}\|}{c^2}, \\ \frac{\partial g_{\tau_i}(\boldsymbol{\beta})}{\partial \mathbf{v}} &= \mathbf{0}, \\ \frac{\partial g_{\rho_i}(\boldsymbol{\beta})}{\partial \mathbf{x}_{\tau_0}} &= \frac{1}{c}\left(\frac{(\mathbf{v}_0 - \mathbf{v})}{\|\mathbf{x}_0 - \mathbf{x}_{\tau_0}\|} + \frac{(\mathbf{v}_i - \mathbf{v})}{\|\mathbf{x}_i - \mathbf{x}_{\tau_0}\|}\right), \end{aligned} \tag{45}$$

$$\frac{\partial g_{\rho_i}(\boldsymbol{\beta})}{\partial c} = \frac{1}{c^2}\left(v_0 + v_i\right),$$
$$\frac{\partial g_{\rho_i}(\boldsymbol{\beta})}{\partial \mathbf{v}} = \frac{1}{c}\left(\frac{(\mathbf{x}_0 - \mathbf{x}_{\tau_0})}{\|\mathbf{x}_0 - \mathbf{x}_{\tau_0}\|} + \frac{(\mathbf{x}_i - \mathbf{x}_{\tau_0})}{\|\mathbf{x}_i - \mathbf{x}_{\tau_0}\|}\right).$$

APPENDIX C
OPTIMAL WEIGHT MATRIX $\mathbf{W}$

Suppose we have an observation equation expressed by

$$\mathbf{y} = \mathbf{H}\mathbf{x} + \mathbf{n}. \tag{46}$$

And we want to estimate $\mathbf{x}$ by a linear estimator defined as

$$\hat{\mathbf{x}} = \mathbf{A}\mathbf{y} + \mathbf{b}. \tag{47}$$

Now, we want to minimize the fitting error of $\mathbf{x}$ with an unbias estimation, which can be formed as follow,

$$\begin{aligned} \text{min.} \quad & \mathbb{E}_{\mathbf{n}}\left\{\|\mathbf{A}\mathbf{y} + \mathbf{b} - \mathbf{x}\|^2\right\} \\ \text{s.t.} \quad & \mathbf{A}\mathbf{H} = \mathbf{I} \end{aligned} \tag{48}$$

Based on Karush-Kuhn-Tucker (K.K.T.) condition, the Lagrangian function can be expressed as

$$\mathcal{L}(\mathbf{A}, \mathbf{b}, \boldsymbol{\Lambda}) = \mathbb{E}_{\mathbf{n}}\left\{\|\mathbf{A}\mathbf{y} + \mathbf{b} - \mathbf{x}\|^2\right\} - \text{Tr}\{(\mathbf{A}\mathbf{H} - \mathbf{I})\boldsymbol{\Lambda}^T\}. \tag{49}$$

The optimal solution of (48) should satisfy

$$\nabla_{\mathbf{A}}\mathcal{L} = \mathbb{E}_{\mathbf{n}}\{2(\mathbf{A}\mathbf{y} + \mathbf{b} - \mathbf{x})\mathbf{y}^T\} + \boldsymbol{\Lambda}\mathbf{H}^T = \mathbf{0}, \tag{50a}$$
$$\nabla_{\mathbf{b}}\mathcal{L} = \mathbb{E}_{\mathbf{n}}\{2(\mathbf{A}\mathbf{y} + \mathbf{b} - \mathbf{x})\} = \mathbf{0}, \tag{50b}$$
$$\nabla_{\boldsymbol{\Lambda}}\mathcal{L} = \mathbf{A}\mathbf{H} - \mathbf{I} = \mathbf{0}. \tag{50c}$$

From (50b), we have

$$\mathbf{b} = -\mathbf{A}\mathbb{E}\{\mathbf{n}\}. \tag{51}$$

Substituting (51) to (50a), we have

$$2\mathbf{A}\mathbf{R}_{\mathbf{n},\mathbf{n}} + \boldsymbol{\Lambda}\mathbf{H}^T = \mathbf{0}, \tag{52}$$

where $\mathbf{R}_{\mathbf{n},\mathbf{n}} = \mathbb{E}\{\mathbf{n}\mathbf{n}^T\} - \mathbb{E}\{\mathbf{n}\}\mathbb{E}\{\mathbf{n}^T\}$. Then, from (52), we can get

$$\mathbf{A} = -\frac{1}{2}\boldsymbol{\Lambda}\mathbf{H}^T\mathbf{R}_{\mathbf{n},\mathbf{n}}^{-1}. \tag{53}$$

After substituting (53) to (50c), we have

$$\boldsymbol{\Lambda} = -2\left(\mathbf{H}^T\mathbf{R}_{\mathbf{n},\mathbf{n}}^{-1}\mathbf{H}\right)^{-1}. \tag{54}$$

Substituting (54) to (52), we get

$$\mathbf{A} = \left(\mathbf{H}^T\mathbf{R}_{\mathbf{n},\mathbf{n}}^{-1}\mathbf{H}\right)^{-1}\mathbf{H}^T\mathbf{R}_{\mathbf{n},\mathbf{n}}^{-1}. \tag{55}$$

According to (29) and (47), we can conclude that $\mathbf{W} = \mathbf{R}_{\mathbf{n},\mathbf{n}}^{-1}$.

APPENDIX D
PROOF OF (37)

To prove (37), we prefer to prove that each element in $\boldsymbol{\Sigma}$ equals to 0. We first rewrite (1) and (4) using the first-order Taylor expansion. Then, we discuss $\sigma_{\tau_i}^2$ and $\sigma_{\rho_i}^2$, respectively.

Let $\mathfrak{f} = \|\mathbf{x}_0 - \mathbf{x}_{\tau_0}\|$, $\mathfrak{g} = \|\mathbf{x}_i + \mathbf{v}_i\tau_i - \mathbf{x}_{\tau_0}\|$, and $\mathfrak{h} = c\tau_i$, then (4) can be rewritten as $\mathfrak{f} + \mathfrak{g} = \mathfrak{h}$. We derive the first order Taylor expansion of $\mathfrak{f}$, $\mathfrak{g}$, and $\mathfrak{h}$ at $\tau_i = \bar{\tau}_i$, $\mathbf{x}_{\tau_0} = \bar{\mathbf{x}}_{\tau_0}$, and $c = \bar{c}$, respectively. Hereafter, we can reorganize (4) as follows,

$$\tau_i = \frac{\mathbb{F} + \mathbb{G} + \mathbb{H}}{\bar{c} - \mathcal{G}}, \tag{56}$$

where $\mathbb{F} = \mathfrak{f}(\bar{\mathbf{x}}_{\tau_0}) + (\nabla_{\mathbf{x}_{\tau_0}}\mathfrak{f})^T(\mathbf{x}_{\tau_0} - \bar{\mathbf{x}}_{\tau_0}), \mathbb{G} = \mathfrak{g}(\bar{\mathbf{x}}_{\tau_0}, \bar{\tau}_i) + (\nabla_{\mathbf{x}_{\tau_0}}\mathfrak{g})^T(\mathbf{x}_{\tau_0} - \bar{\mathbf{x}}_{\tau_0}), \mathbb{H} = -\bar{\tau}_i(c - \bar{c} + \mathcal{G}), \quad \mathcal{G} = \partial\mathfrak{g}/\partial\tau_i$. Therefore,

$$\sigma_{\tau_i}^2 = \frac{\left(\|\nabla_{\mathbf{x}_{\tau_0}}\mathfrak{f}\|^2 + \|\nabla_{\mathbf{x}_{\tau_0}}\mathfrak{g}\|^2\right)\sigma_{\mathbf{x}_{\tau_0}}^2 - \bar{\tau}_i{}^2\sigma_c^2}{(\bar{c} - \mathcal{G})^2}. \tag{57}$$

We have

$$\frac{\partial\sigma_{\tau_i}^2}{\partial\mathbf{v}} = \mathbf{0}, \frac{\partial\sigma_{\tau_i}}{\partial\mathbf{v}} = \mathbf{0}. \tag{58}$$

We also have

$$\frac{\partial\sigma_{\tau_i}^2}{\partial\mathbf{x}_{\tau_0}} = \frac{\left(\|\nabla_{\mathbf{x}_{\tau_0}}\mathfrak{f}\|^2 + \|\nabla_{\mathbf{x}_{\tau_0}}\mathfrak{g}\|^2\right)}{(\bar{c} - \mathcal{G})^2}\frac{\partial\sigma_{\mathbf{x}_{\tau_0}}^2}{\partial\mathbf{x}_{\tau_0}}, \tag{59}$$

and

$$\frac{\partial\sigma_{\tau_i}^2}{\partial c} = \frac{-\bar{\tau}_i{}^2}{(\bar{c} - \mathcal{G})^2}\frac{\partial\sigma_c^2}{\partial c}. \tag{60}$$

Moreover, we have

$$\|\nabla_{\mathbf{x}_{\tau_0}}\mathfrak{f}\|^2 = 1, \tag{61}$$
$$\|\nabla_{\mathbf{x}_{\tau_0}}\mathfrak{g}\|^2 = 1, \tag{62}$$

and

$$\mathcal{G} = \|\mathbf{v}\|. \tag{63}$$

We observe that $\|\mathbf{v}_i\| \ll \bar{c}$. Therefore, $(\|\nabla_{\mathbf{x}_{\tau_0}}\mathfrak{f}\|^2 + \|\nabla_{\mathbf{x}_{\tau_0}}\mathfrak{g}\|^2) \ll (\bar{c} - \|\mathbf{v}_i\|)^2$ and $\bar{\tau}_i{}^2 \ll (\bar{c} - \|\mathbf{v}_i\|)^2$. Consequently,

$$\frac{\partial\sigma_{\tau_i}^2}{\partial\mathbf{x}_{\tau_0}} \approx \mathbf{0}, \frac{\partial\sigma_{\tau_i}^2}{\partial c} \approx 0, \tag{64}$$
$$\frac{\partial\sigma_{\tau_i}}{\partial\mathbf{x}_{\tau_0}} \approx \mathbf{0}, \frac{\partial\sigma_{\tau_i}}{\partial c} \approx 0. \tag{65}$$

Similar with (56), let $\mathfrak{f} = \rho_i(\mathbf{v}_i - \mathbf{v})^T\frac{(\mathbf{x}_i - \mathbf{x}_{\tau_0})}{\|\mathbf{x}_i - \mathbf{x}_{\tau_0}\|}$, $\mathfrak{g} = (\mathbf{v}_0 - \mathbf{v})^T\frac{(\mathbf{x}_0 - \mathbf{x}_{\tau_0})}{\|\mathbf{x}_0 - \mathbf{x}_{\tau_0}\|}$, and $\mathfrak{h} = c(1 - \rho_i)$. Then, we can rewrite (1) as $\mathfrak{f} + \mathfrak{g} = \mathfrak{h}$. We derive the first order Taylor expansion of $\mathfrak{f}$, $\mathfrak{g}$, and $\mathfrak{h}$ at $\rho_i = \bar{\rho}_i$, $\mathbf{x}_{\tau_0} = \bar{\mathbf{x}}_{\tau_0}$, and $\mathbf{v} = \bar{\mathbf{v}}$, respectively. Hereafter, we can reorganize (1) as

$$\rho_i = \frac{\mathbb{F} + \mathbb{G} + \mathbb{H}}{(-\mathcal{F} - \bar{c})}, \tag{66}$$

where $\mathbb{F} = \mathfrak{f}(\bar{\rho}_i, \bar{\mathbf{x}}_{\tau_0}, \bar{\mathbf{v}}) + (\nabla_{\mathbf{x}_{\tau_0}}\mathfrak{f})^T(\mathbf{x}_{\tau_0} - \bar{\mathbf{x}}_{\tau_0}) + (\nabla_{\mathbf{v}}\mathfrak{f})^T(\mathbf{v} - \bar{\mathbf{v}}) - \mathcal{F}\bar{\rho}_i, \quad \mathbb{G} = \mathfrak{g}(\bar{\mathbf{x}}_{\tau_0}, \bar{\mathbf{v}}) + (\nabla_{\mathbf{x}_{\tau_0}}\mathfrak{g})^T(\mathbf{x}_{\tau_0} - \bar{\mathbf{x}}_{\tau_0}) + (\nabla_{\mathbf{v}}\mathfrak{g})^T(\mathbf{v} - \bar{\mathbf{v}}), \quad \mathbb{H} = -\bar{c}(1 - \bar{\rho}_i) - (1 - \bar{\rho}_i)(c - \bar{c}) - \bar{c}\bar{\rho}_i$, and $\mathcal{F} = \partial\mathfrak{f}/\partial\rho_i$. Then, we have

$$\sigma_{\rho_i}^2 = \frac{\|\nabla_{\mathbf{x}_{\tau_0}}\mathfrak{f}\|^2 + \|\nabla_{\mathbf{x}_{\tau_0}}\mathfrak{g}\|^2}{(-\mathcal{F} - \bar{c})^2}\sigma_{\mathbf{x}_{\tau_0}}^2$$

$$+\frac{\|\nabla_{\mathbf{v}}\mathfrak{f}\|^2+\|\nabla_{\mathbf{v}}\mathfrak{g}\|^2}{(-\mathcal{F}-\bar{c})^2}\sigma_{\mathbf{v}}^2 - \frac{(1-\bar{\rho}_i)^2}{(\mathcal{F}-\bar{c})^2}\sigma_c^2. \quad (67)$$

Let $\Delta v_{i,x}=v_{i,x}-v_x$, $\Delta v_{i,y}=v_{i,y}-v_y$, $\Delta x_{i,x}=x_{i,x}-x_{\tau_0,x}$, and $\Delta x_{i,y}=x_{i,y}-x_{\tau_0,y}$. We have

$$\frac{\partial\mathfrak{f}}{\partial x_{\tau_0,x}}=-\rho_i\left(\frac{\Delta x_{i,y}\left(\frac{\Delta x_{i,x}}{\tau_i}\Delta x_{i,y}-\frac{\Delta x_{i,y}}{\tau_i}\Delta x_{i,x}\right)}{\|\mathbf{x}_i-\mathbf{x}_{\tau_0}\|^3}\right) =0. \quad (68)$$

Similarly, $\partial\mathfrak{f}/\partial x_{\tau_0,y}=0$. Thus, $\|\nabla_{\mathbf{x}_{\tau_0}}\mathfrak{f}\|=0$. Following the same approach, $\|\nabla_{\mathbf{x}_{\tau_0}}\mathfrak{g}\|=0$. Therefore, we have

$$\frac{\partial\sigma_{\rho_i}^2}{\partial\mathbf{x}_{\tau_0}}\approx\mathbf{0},\ \frac{\partial\sigma_{\rho_i}}{\partial\mathbf{x}_{\tau_0}}\approx\mathbf{0}. \quad (69)$$

Moreover,

$$\|\nabla_{\mathbf{v}}\mathfrak{f}\|^2=\left(\bar{\rho_i}^2\frac{(x_{i,x}-x_{\tau_0,x})^2+(x_{i,y}-x_{\tau_0,y})^2}{\|\mathbf{x}_i-\mathbf{x}_{\tau_0}\|^2}\right) =\left(\bar{\rho_i}^2\frac{\Delta x_{i,x}^2+\Delta x_{i,y}^2}{\Delta x_{i,x}^2+\Delta x_{i,y}^2}\right) =\bar{\rho_i}^2. \quad (70)$$

Similarly, we have $\|\nabla_{\mathbf{v}}\mathfrak{g}\|^2=\bar{\rho_i}^2$. Moreover,

$$\mathcal{F}=\left((\mathbf{v}_i-\mathbf{v})^T\frac{(\mathbf{x}_i-\mathbf{x}_{\tau_0})}{\|\mathbf{x}_i-\mathbf{x}_{\tau_0}\|}\right)\ll\bar{c}. \quad (71)$$

Therefore, $\|\nabla_{\mathbf{v}}\mathfrak{f}\|^2+\|\nabla_{\mathbf{v}}\mathfrak{g}\|^2\ll(-\mathcal{F}-\bar{c})^2$. We have

$$\frac{\partial\sigma_{\rho_i}^2}{\partial\mathbf{v}}\approx\mathbf{0},\ \frac{\partial\sigma_{\rho_i}}{\partial\mathbf{v}}\approx\mathbf{0}. \quad (72)$$

Furthermore, $(1-\bar{\rho}_i)^2\ll(\mathcal{F}-\bar{c})^2$. Therefore, we have

$$\frac{\partial\sigma_{\rho_i}^2}{\partial c}\approx 0,\ \frac{\partial\sigma_{\rho_i}}{\partial c}\approx 0. \quad (73)$$

In addition,

$$\frac{\partial\mathrm{cov}(\tau_i,\rho_i)}{\partial\boldsymbol{\beta}[i]}\approx 0. \quad (74)$$

Consequently, we have

$$\frac{1}{2}\mathrm{Tr}\left(\boldsymbol{\Sigma}^{-1}\frac{\partial\boldsymbol{\Sigma}}{\partial\boldsymbol{\beta}[i]}\boldsymbol{\Sigma}^{-1}\frac{\partial\boldsymbol{\Sigma}}{\partial\boldsymbol{\beta}[j]}\right)\approx 0. \quad (75)$$

REFERENCES

[1] F. Tang, B. Mao, Y. Kawamoto, and N. Kato, "Survey on machine learning for intelligent end-to-end communication toward 6G: From network access, routing to traffic control and streaming adaption," *IEEE Commun. Surv. Tut.*, vol. 23, no. 3, pp. 1578–1598, Jul–Sep. 2021.

[2] T. Hong, M. Lv, S. Zheng, and H. Hong, "Key technologies in 6G SAGS IoT: Shape-adaptive antenna and radar-communication integration," *IEEE Netw.*, vol. 35, no. 5, pp. 150–157, Sep./Oct. 2021.

[3] Y. Liu, C.-X. Wang, H. Chang, Y. He, and J. Bian, "A novel non-stationary channel model for maritime communications," *IEEE J. Sel. Areas Commun.*, vol. 39, no. 10, pp. 2992–3005, Oct. 2021.

[4] X. Wang, H. Lin, H. Zhang, D. Miao, Q. Miao, and W. Liu, "Intelligent drone-assisted fault diagnosis for -enabled space-air-ground-space networks," *IEEE Trans. Netw. Sci. Eng.*, vol. 8, no. 4, pp. 2849–2860, Oct.–Dec. 2021.

[5] H. Guo, J. Li, J. Liu, N. Tian, and N. Kato, "A survey on space-air-ground-sea integrated network security in 6G," *IEEE Commun. Surv. Tut.*, vol. 24, no. 1, pp. 53–87, Jan.–Mar. 2022.

[6] A. Song, M. Stojanovic, and M. Chitre, "Editorial underwater acoustic communications: Where we stand and what is next?," *IEEE J. Ocean. Eng.*, vol. 44, no. 1, pp. 1–6, Jan. 2019.

[7] D. A. Abraham, *Underwater Acoustic Signal Processing*. Cham, Switzerland: Springer, 2019.

[8] X. Pan, Y. Shen, and J. Zhang, "IoUT based underwater target localization in the presence of time synchronization attacks," *IEEE Trans. Wireless Commun.*, vol. 20, no. 6, pp. 3958–3973, Jun. 2021.

[9] I. S. Kulkarni and D. Pompili, "Task allocation for networked autonomous underwater vehicles in critical missions," *IEEE J. Sel. Areas Commun.*, vol. 28, no. 5, pp. 716–727, Jun. 2010.

[10] B. Chen and D. Pompili, "A QoS-aware underwater optimization framework for inter-vehicle communication using acoustic directional transducers," *IEEE Trans. Wireless Commun.*, vol. 13, no. 5, pp. 2490–2504, May 2014.

[11] X. Cao, D. Zhu, and S. X. Yang, "Multi-AUV target search based on bioinspired neurodynamics model in 3-D underwater environments," *IEEE Trans. Neural Netw. Learn. Syst.*, vol. 27, no. 11, pp. 2364–2374, Nov. 2016.

[12] S. F. Mason, C. R. Berger, S. Zhou, and P. Willett, "Detection, synchronization, and Doppler scale estimation with multicarrier waveforms in underwater acoustic communication," *IEEE J. Sel. Areas Commun.*, vol. 26, no. 9, pp. 1638–1649, Dec. 2008.

[13] Y. Shen, H. Wymeersch, and M. Z. Win, "Fundamental limits of wideband localization- part II: Cooperative networks," *IEEE Trans. Inf. Theory*, vol. 56, no. 10, pp. 4981–5000, Oct. 2010.

[14] Y. Li, L. Liu, W. Yu, Y. Wang, and X. Guan, "Noncooperative mobile target tracking using multiple AUVs in anchor-free environments," *IEEE Internet Things J.*, vol. 7, no. 10, pp. 9819–9833, Oct. 2020.

[15] T. K. Rodrigues, J. Liu, and N. Kato, "Offloading decision for mobile multi-access edge computing in a multi-tiered 6G network," *IEEE Trans. Emerg. Topics Comput.*, vol. 10, no. 3, pp. 1414–1427, Jul./Sep. 2022.

[16] P. A. Miller, J. A. Farrell, Y. Zhao, and V. Djapic, "Autonomous underwater vehicle navigation," *IEEE J. Ocean. Eng.*, vol. 35, no. 3, pp. 663–678, Jul. 2010.

[17] S. Hara, D. Anzai, T. Yabu, K. Lee, T. Derham, and R. Zemek, "A perturbation analysis on the performance of TOA and TDOA localization in mixed LOS/NLOS environments," *IEEE Trans. Commun.*, vol. 61, no. 2, pp. 679–689, Feb. 2013.

[18] R. Diamant and L. Lampe, "Underwater localization with time-synchronization and propagation speed uncertainties," *IEEE Trans. Mobile Comput.*, vol. 12, no. 7, pp. 1257–1269, Jul. 2013.

[19] Z. Gong, C. Li, and F. Jiang, "AUV-aided joint localization and time synchronization for underwater acoustic sensor networks," *IEEE Signal Process. Lett.*, vol. 25, no. 4, pp. 477–481, Apr. 2018.

[20] J. Yan, X. Zhang, X. Luo, Y. Wang, C. Chen, and X. Guan, "Asynchronous localization with mobility prediction for underwater acoustic sensor networks," *IEEE Trans. Veh. Technol.*, vol. 67, no. 3, pp. 2543–2556, Mar. 2018.

[21] P. C. Etter, *Underwater Acoustic Modeling and Simulation*, 5th ed. Boca Raton, FL, USA: CRC Press, Taylor & Francis Group, 2018.

[22] H. Ramezani, H. Jamali-Rad, and G. Leus, "Target localization and tracking for an isogradient sound speed profile," *IEEE Trans. Signal Process.*, vol. 61, no. 6, pp. 1434–1446, Mar. 2013.

[23] T. K. Rodrigues, K. Suto, and N. Kato, "Edge cloud server deployment with transmission power control through machine learning for 6G Internet of Things," *IEEE Trans. Emerg. Topics Comput.*, vol. 9, no. 4, pp. 2099–2108, Oct.–Dec. 2021.

[24] D. Park, K. Kwak, W. K. Chung, and J. Kim, "Development of underwater short-range sensor using electromagnetic wave attenuation," *IEEE J. Ocean. Eng.*, vol. 41, no. 2, pp. 318–325, Apr. 2016.

[25] Z. Gong, C. Li, F. Jiang, and J. Zheng, "AUV-aided localization of underwater acoustic devices based on doppler shift measurements," *IEEE Trans. Wireless Commun.*, vol. 19, no. 4, pp. 2226–2239, Apr. 2020.

[26] Z. Gong, C. Li, and F. Jiang, "A machine learning-based approach for auto-detection and localization of targets in underwater acoustic array networks," *IEEE Trans. Veh. Technol.*, vol. 69, no. 12, pp. 15857–15866, Dec. 2020.

[27] J. R. Bates, S. M. Murphy, B. H. Maranda, and D. A. Abraham, "Signal-to-reverberation ratio comparison of linear frequency modulated continuous active sonar and pulsed active sonar," *IEEE J. Ocean. Eng.*, vol. 46, no. 2, pp. 654–664, Apr. 2021.
[28] R. Van Vossen, S. P. Beerens, and E. van der Spek, "Anti-submarine warfare with continuously active sonar," *Sea Technol.*, vol. 52, no. 11, pp. 33–35, 2011.
[29] J. Liang, L. Xu, J. Li, and P. Stoica, "On designing the transmission and reception of multistatic continuous active sonar systems," *IEEE Trans. Aerosp. Electron. Syst.*, vol. 50, no. 1, pp. 285–299, Jan. 2014.
[30] Y. Zhao, H. Yu, G. Wei, F. Ji, and F. Chen, "Parameter estimation of wide-band underwater acoustic multipath channels based on fractional fourier transform," *IEEE Trans. Signal Process.*, vol. 64, no. 20, pp. 5396–5408, Oct. 2016.
[31] L. B. Almeida, "The fractional fourier transform and time-frequency representations," *IEEE Trans. Signal Process.*, vol. 42, no. 11, pp. 3084–3091, Nov. 1994.
[32] K. Zhao, J. Liang, J. Karlsson, and J. Li, "Enhanced multistatic active sonar signal processing," *J. Acoustical Soc. Amer.*, vol. 134, no. 1, pp. 300–311, Jul. 2013.
[33] A. Amar, G. Leus, and B. Friedlander, "Emitter localization given time delay and frequency shift measurements," *IEEE Trans. Aerosp. Electron. Syst.*, vol. 48, no. 2, pp. 1826–1837, Apr. 2012.
[34] M. Stojanovic and J. Preisig, "Underwater acoustic communication channels: Propagation models and statistical characterization," *IEEE Commun. Mag.*, vol. 47, no. 1, pp. 84–89, Jan. 2009.
[35] Z. Gong, C. Li, and F. Jiang, "Analysis of the underwater multi-path reflections on shift estimation," *IEEE Wireless Commun. Lett.*, vol. 9, no. 10, pp. 1758–1762, Oct. 2020.
[36] K. Conrad, "Probability distributions and maximum entropy," *Entropy*, vol. 6, no. 452, pp. 1–27, 2004.
[37] S. Guiasu and A. Shenitzer, "The principle of maximum entropy," *Math. Intelligencer*, vol. 7, no. 1, pp. 42–48, 1985.
[38] L. Malagó and G. Pistone, "Information geometry of the Gaussian distribution in view of stochastic optimization," in *Proc. ACM Conf. Found. Genet. Algorithms XIII*, 2015, pp. 150–162.

Ruoyu Su received the B.Eng. and M.Eng. degrees from the Nanjing University of Aeronautics and Astronautics, Nanjing, China, in 2006 and 2009, respectively, and the Ph.D. degree in electrical and computer engineering from the Memorial University of Newfoundland, St. John's, NL, Canada, in 2015. He completed the Postdoctoral work in 2016 with the Department of Electrical and Computer Engineering, Memorial University of Newfoundland. From 2016 to 2018, he was a Software Engineer with Huawei Shanghai Research Institute. He is currently with the Nanjing University of Posts and Telecommunications, Nanjing, China. His research interests include signal processing and localization, energy-efficient design for Internet of underwater things, and 5G network slicing.

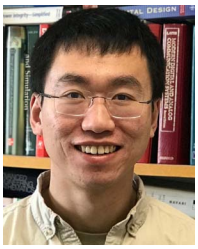

Zijun Gong (Member, IEEE) received the B.Eng. and M.Eng. degrees from the Harbin Institute of Technology, Harbin, China, in 2013 and 2015, respectively, and the Ph.D. degree from the Memorial University of Newfoundland, St. John's, NL, Canada, in 2021. From May 2021 to December 2021, he was with the University of Waterloo, Waterloo, ON, Canada, as a Postdoctoral Researcher. He is currently an Assistant Professor with the IoT Thrust in Information Hub, The Hong Kong University of Science and Technology (Guangzhou), Guangzhou, China. He is also an affiliate Assistant Professor with the ECE Department, Hong Kong University of Science and Technology, Hong Kong. His research interests lie in statistical signal processing and optimization, including channel estimation in massive MIMO, and millimeter wave communications, mmWave radar, radio propagation modeling, localization of WSN, and localization of underwater targets and devices. He was the recipient of the Best Paper Award at the IEEE GLOBECOM'17, Singapore, in December 2017.

Cheng Li (Senior Member, IEEE) received the B.Eng. and M.Eng. degrees from the Harbin Institute of Technology, Harbin, China, 1992 and 1995, respectively, and the Ph.D. degree in electrical and computer engineering from Memorial University of Newfoundland, St. John's, NL, Canada, in 2004. He is currently the Head and a Full Professor with the Department of Electrical and Computer Engineering, Memorial University of Newfoundland. His research interests include wireless communications and networking, mobile computing, underwater communications and networks, Internet-of-Things, and broadband communication networks. He is a Registered Professional Engineer in Canada and a Senior Member of the IEEE and its Communications, Computer, Ocean Engineering, and Vehicular Technology Societies. He was the recipient of the Best Paper Award at the International Conference on Ad Hoc Networks (ADHOCNETS) 2018, the IEEE Global Communications Conference 2017, and the IEEE International Conference on Communications 2010. He is an Associate Editor for IEEE INTERNET-OF-THINGS JOURNAL, IEEE NETWORK MAGAZINE, IEEE SYSTEM JOURNAL, and *China Communications*. He was the General Co-Chair of the ICNC'22, AICON'19, WINCOM'19 in WINCOM'17 and TPC Co-Chair of the ICNC'20, ADHOCNETS'19, ADHOCNETS'17, MSWiM'14, MSWiM'13, WINCOM'11, and QBSC'10. He was the Co-Chair of various technical symposia or tracks of many international conferences, including the IEEE International Conference on Communications, IEEE Global Communications Conference, IEEE International Conference on Neuromorphic Computing, IEEE Conference on Vehicular Technology, and IEEE International Wireless Communications and Mobile Computing Conference.

Xuemin (Sherman) Shen (Fellow, IEEE) received the Ph.D. degree in electrical engineering from Rutgers University, New Brunswick, NJ, USA, in 1990. He is currently a University Professor with the Department of Electrical and Computer Engineering, University of Waterloo, Waterloo, ON, Canada. His research interests include network resource management, wireless network security, Internet of Things, 5G and beyond, and vehicular networks. He is a registered Professional Engineer of Ontario, Canada, an Engineering Institute of Canada Fellow, a Canadian Academy of Engineering Fellow, a Royal Society of Canada Fellow, a Chinese Academy of Engineering Foreign Member, and a Distinguished Lecturer of the IEEE Vehicular Technology Society and Communications Society. Dr. Shen was the recipient of the Canadian Award for Telecommunications Research from the Canadian Society of Information Theory in 2021, R.A. Fessenden Award in 2019 from IEEE, Canada, Award of Merit from the Federation of Chinese Canadian Professionals (Ontario) in 2019, James Evans Avant Garde Award in 2018 from the IEEE Vehicular Technology Society, Joseph LoCicero Award in 2015 and Education Award in 2017 from the IEEE Communications Society (ComSoc), and Technical Recognition Award from Wireless Communications Technical Committee (2019) and AHSN Technical Committee (2013). He was also the recipient of the Excellent Graduate Supervision Award in 2006 from the University of Waterloo and the Premier's Research Excellence Award in 2003 from the Province of Ontario, Canada. He was the Technical Program Committee Chair/Co-Chair for IEEE Globecom'16, IEEE Infocom'14, IEEE VTC'10 Fall, IEEE Globecom'07, and Chair for the IEEE ComSoc Technical Committee on Wireless Communications. He is the President of the IEEE Communications Society (ComSoc). He was the Vice President of Technical and Educational Activities, Vice President of Publications, a Member-at-Large on the Board of Governors, the Chair of the Distinguished Lecturer Selection Committee, and a Member of IEEE Fellow Selection Committee of the ComSoc. He was the Editor-in-Chief of the IEEE INTERNET OF THINGS JOURNAL, IEEE NETWORK, and *IET Communications*.